Physics Letters A 379 (2015) 894–900

Contents lists available at ScienceDirect

Physics Letters A

www.elsevier.com/locate/pla

Analysing spatially extended high-dimensional dynamics by recurrence plots

Norbert Marwan [a,*], Jürgen Kurths [a,b,c], Saskia Foerster [d]

[a] Potsdam Institute for Climate Impact Research, 14412 Potsdam, Germany
[b] Humboldt Universität zu Berlin, Institut für Physik, Germany
[c] Nizhny Novgorod State University, Department of Control Theory, Nizhny Novgorod, Russia
[d] GFZ German Research Centre for Geosciences, Section 1.4 Remote Sensing, Telegrafenberg, 14473 Potsdam, Germany

ARTICLE INFO

Article history:
Received 20 November 2014
Received in revised form 14 January 2015
Accepted 16 January 2015
Available online 20 January 2015
Communicated by C.R. Doering

Keywords:
Spatially extended chaos
Recurrence plot
Lorenz96
Remote sensing

ABSTRACT

Recurrence plot based measures of complexity are capable tools for characterizing complex dynamics. In this letter we show the potential of selected recurrence plot measures for the investigation of even high-dimensional dynamics. We apply this method on spatially extended chaos, such as derived from the Lorenz96 model and show that the recurrence plot based measures can qualitatively characterize typical dynamical properties such as chaotic or periodic dynamics. Moreover, we demonstrate its power by analysing satellite image time series of vegetation cover with contrasting dynamics as a spatially extended and potentially high-dimensional example from the real world.

1. Introduction

The recurrence plot (RP) is a modern and versatile tool for the study of the complex behavior of dynamical systems [1,2]. It represents time points of recurring states even of high-dimensional phase space trajectories. Quantitative extensions, such as recurrence quantification analysis and recurrence networks, enable the investigation of dynamical transitions and regime changes, the quantitative characterization of the dynamics, or the detection of phase synchronization [3–5]. As proven by several examples, the RP based quantities work quite well even with short time series (e.g., [6–9]). The practical and powerful use of RP based methods has been demonstrated by their growing and interdisciplinary application, such as for cardiovascular health diagnosis, behavioral, cognitive and neurological studies, studying fluid dynamics and plasma, analysing optical effects, material health monitoring, palaeoclimate regime change detection, etc. [9–16]. In general, such studies have so far been restricted to rather low-dimensional systems. However, when studying the complex behavior of real world systems, we often end up with extended complex systems, and the question arises whether the RP based tools can be applied on high-dimensional systems, such as exhibiting high-dimensional chaos. So far, the ability of RP based methods for studying high-dimensional dynamics has not yet been demonstrated, although it was already used to investigate spatial recurrences [17–19] and spatio-temporal chaos in turbulence and a reaction–diffusion system [20,21]. Moreover, the classic characterization of complex dynamics by using, e.g., entropy [22], correlation dimension [23], and Lyapunov exponents requires very long time-series [24] or the knowledge of the differential equations of the system which are in practical examples not known. The study of extended spatio-temporal dynamics is even more challenging because of the large degrees of freedom.

In this letter we demonstrate the potential of RP based measures of complexity for identifying hardly accessible extended spatio-temporal dynamics and for characterizing high-dimensional chaos. We will use the Lorenz96 model [25–27] which is a paradigmatic system for extended complex spatio-temporal chaotic dynamics and was systematically studied by Karimi et al. [28] and apply the method on an example of a satellite time series imagery.

2. The Lorenz96 model

The Lorenz96 model is a conceptual time-continuous linear lattice model that was developed to demonstrate fundamental aspects of weather predictability [25]:

$$\frac{dx_k}{dt} = (x_{k+1} - x_{k-2})x_{k-1} - x_{k-1} + f \tag{1}$$

* Corresponding author.
E-mail address: marwan@pik-potsdam.de (N. Marwan).

http://dx.doi.org/10.1016/j.physleta.2015.01.013
0375-9601/

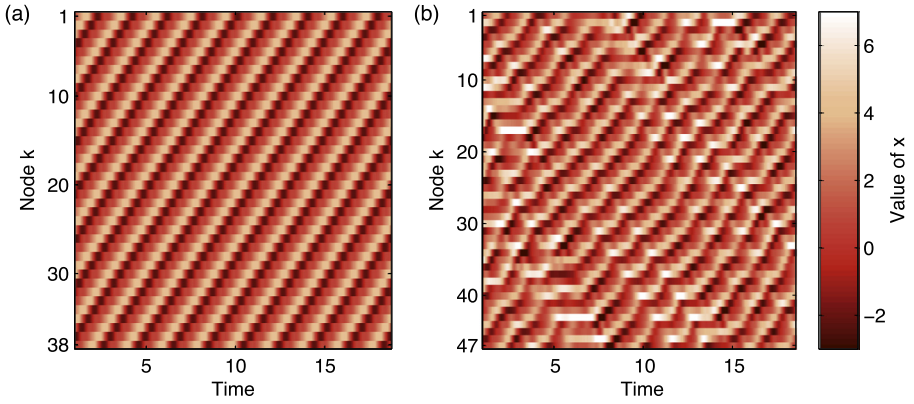

Fig. 1. Space–time representation of $x_k(t)$ of the Lorenz96 system, Eq. (1), for $f = 5$ and system size of (a) $N = 38$ and (b) $N = 47$, showing periodic and chaotic dynamics.

for $k = 1, \ldots, N$, with a constant external forcing f, and with periodic boundary conditions $x_{N+1} = x_1$. Depending on the system size N and the forcing f, the dynamics on the lattice can be periodic or chaotic and can exhibit a high dimensionality [28]. Therefore, this model is very appropriate for our study.

For integrating Eq. (1) we use a Runge–Kutta integration of 4th order with time step $\delta t = 1/64$. In order to remove transients, we neglect the first 10,000 values from each $x_k(t)$. In the numerical experiments discussed below, we will use 20 slightly varying initial conditions for each selected setting of N and f.

In our study we consider $f = 5$ (as used by Karimi et al. [28]). Then, for example, for $N = 38$, we find periodic dynamics, but for $N = 47$, the dynamics is chaotic (Fig. 1).

The change of the dynamical regimes with system size N can be measured by the maximal Lyapunov exponent $\lambda_{\max}$ and the Kaplan–Yorke dimension D_{KY}. Here we compute the Lyapunov spectrum from the set of N differential equations by linearizing the corresponding evolution and using a Gram–Schmidt Orthonormalization scheme [29,30]. For stable results, we integrate 200,000 iterations. The Kaplan–Yorke dimension D_{KY} can then be derived from the N (ordered) Lyapunov exponents by the Kaplan–Yorke algorithm

$$D_{\mathrm{KY}} = K + \sum_{i=1}^{K} \frac{\lambda_i}{|\lambda_{K+1}|}, \tag{2}$$

where K is the largest number of the first largest Lyapunov exponents with $\sum_{i=1}^{K} \lambda_i \geq 0$ [22]. Increasing the system size from $N = 10$ to $N = 50$ reveals a periodic alternation between periodic and chaotic dynamics by periodic variations of $\lambda_{\max}$ (Fig. 2(a)). The dimension of the system dynamics as measured by D_{KY} is increasing by trend (Fig. 3(a)). The calculation of λ and D_{KY} is expensive for such systems with large degrees of freedom. Moreover, for accurate values we need very long time series (here, even for $N = 200{,}000$ we find some spread in the results of $\lambda_{\max}$ and D_{KY}).

3. Recurrence plot analysis

RP quantification may be suitable for a simpler estimation of the dynamical properties. An RP $R_{i,j} = \Theta(\varepsilon - \|\vec{x}_i - \vec{x}_j\|)$ is a binary matrix $\mathbf{R}$ representing the time points j when a state $\vec{x}_i$ at time i recurs [3] (Fig. 4). The recurrence criterion is usually defined as a spatial distance between two states $\vec{x}_i$ and $\vec{x}_j$ is falling below a threshold ε. Besides the ability to discuss the visual aspect of an RP, several quantification approaches are based on this matrix. The diagonal line structures in an RP correspond to periods of parallel evolution of two segments of the phase space trajectory. The scaling of the length distribution of such lines is related to the

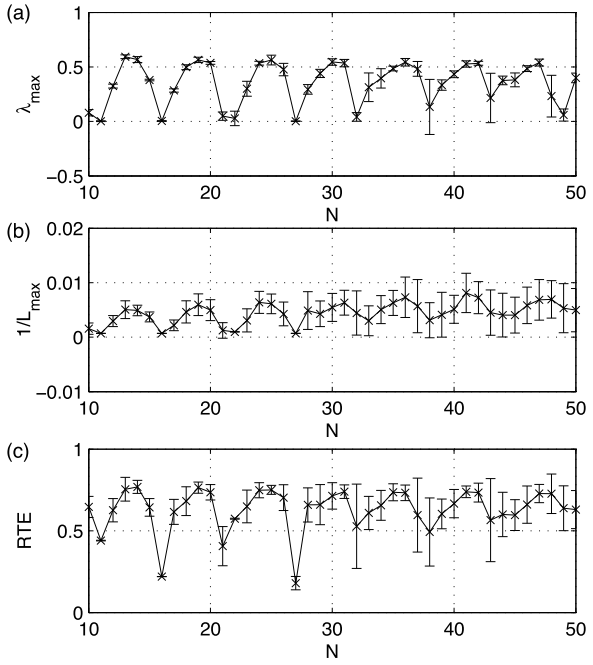

Fig. 2. (a) Maximal Lyapunov exponent $\lambda_{\max}$ for the Lorenz96 system, Eq. (1), with different system size N. The RP based measures (b) $1/L_{\max}$ and (c) RTE reveal a similar variation with the N as $\lambda_{\max}$. Averaged values for 20 different initial states are presented. The standard deviations of the measures for the different initial conditions are presented by the error bars.

K_2 entropy. A good proxy for this is measuring the inverse of the length of the longest diagonal line $1/L_{\max}$, with

$$L_{\max} = \arg\max_{l} H_{\mathrm{D}}(l), \tag{3}$$

and l the length of the diagonal lines, and $H_{\mathrm{D}}(l)$ the length distribution of diagonal lines in $\mathbf{R}$ [3].

Based on a heuristic approach, the fraction of recurrence points that form such diagonal lines is a qualitative measure of predictability, called *determinism (DET)* [3],

$$DET = \frac{\sum_{l=2}^{N} l H_{\mathrm{D}}(l)}{\sum_{i,j=1}^{N} R_{i,j}}. \tag{4}$$

Systems possessing deterministic dynamics are characterized by diagonal lines indicating repeating recurrences within a state (and, hence, higher DET values).

The vertical empty space between two recurrence points in the RP corresponds to Poincaré recurrence times, i.e., the distance v

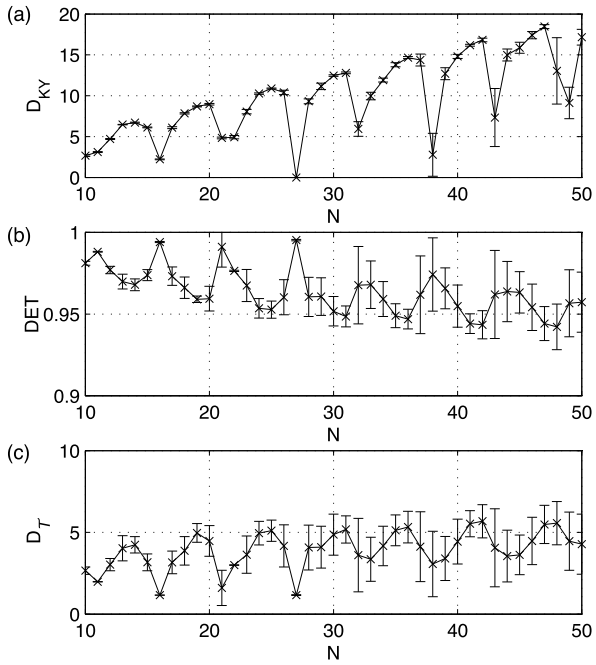

Fig. 3. (a) Kaplan–Yorke dimension D_{KY} for the Lorenz96 system, Eq. (1), with different system size N. The RP based measures (b) DET and (c) $D_{\mathcal{T}}$ reveal a similar variation with the N as D_{KY}. Averaged values for 20 different initial states are presented. The standard deviations of the measures for the different initial conditions are presented by the error bars.

between recurrence points in a column of $\mathbf{R}$ [31]. From the distribution $H_{\mathrm{V}}(v)$ we can derive the *recurrence time entropy (RTE)*, also called *recurrence period density entropy* [32]

$$RTE = -\frac{1}{\ln V_{\max}} \sum_{v=1}^{V_{\max}} H_{\mathrm{V}}(v) \ln H_{\mathrm{V}}(v). \tag{5}$$

This measure quantifies the extent of recurrences and is related to the Pesin dimension [33].

In the last years, the similarity of the binary, squared matrix $\mathbf{R}$ with the adjacency matrix of an unweighted, undirected complex network was used to apply complex network measures on recurrence plots in order to quantify the geometrical properties of the system's attractor encoded in the RP [6]. For example, the *transitivity coefficient* ($\mathcal{T}$)

$$\mathcal{T} = \frac{\sum_{i,j,k=1}^{N} R_{j,k} R_{i,j} R_{i,k}}{\sum_{i,j,k=1}^{N} R_{i,j} R_{i,k} (1 - \delta_{j,k})}, \tag{6}$$

allows the differentiation of periodic and chaotic dynamics [34]. Moreover, $\mathcal{T}$ can be used to define a novel dimensionality measure, the *transitivity dimension* ($D_{\mathcal{T}}$)

$$D_{\mathcal{T}} = \frac{\log(\mathcal{T})}{\log(3/4)}, \tag{7}$$

allowing the calculation of the dimension without explicit consideration of scaling behaviors. Using the RP, the correlation dimension D_2 can also be derived [35]. However, the advantage of $D_{\mathcal{T}}$ is that it results directly from the RP without analysing any scaling behavior depending on the recurrence threshold ε.

Although still rather novel, such recurrence quantification is meanwhile widely accepted and applied in different disciplines to study diverse problems. For more details on this methodology we refer to [3,5,36,37].

4. Recurrence analysis of spatially extended chaos

For the application of the RP approach to spatially extended high-dimensional data such as from the Lorenz96 model, we consider each variable as one component of the phase space representation: $\vec{x}(t) = (x_1(t), x_2(t), \ldots, x_N(t))$. We remove transients by deleting the first 10,000 data points and then downsample the time series by considering only every 2nd value. Then, for only 1500 time points of the vector $\vec{x}(t)$ we calculate the RP and the above mentioned measures DET, $1/L_{\max}$, RTE, and $D_{\mathcal{T}}$. We calculate this set of measures for different system size $N \in \{10, \ldots, 50\}$ and repeat the calculation for 20 different initial conditions. For the line based RP measures DET and $1/L_{\max}$ we choose a minimal line length of two. We apply a Theiler window of length 20 (in units of iteration steps) and a recurrence threshold such that the fraction of recurrences in the RP is 10% (and using the Euclidean norm). We estimated the size of the Theiler window by the autocorrelation time, which is in average 20. The choice of the fixed recurrence rate for the threshold selection is justified by the increase of the state space dimension with growing N that would require a rescaling of the recurrence threshold. By fixing the recurrence rate we can avoid this rescaling.

The inverse of the longest diagonal line $1/L_{\max}$ as well as the RTE reveal a similar alternating variation with N as $\lambda_{\max}$ (Fig. 2(b,c)). The Pearson correlation between these two RP based measures and $\lambda_{\max}$ is 0.745 (for $1/L_{\max}$) and 0.750 (for RTE). The strong correlation even for the used rather short data segment suggests that these RP based measures are good estimators for studying the divergence behavior of high-dimensional systems.

The DET measure varies between values of 0.94 and 1, indicating the deterministic nature of the model (Fig. 3(b)). During the periodic regimes, the DET shows maxima, whereas during the chaotic regime, DET falls to lower values. The transitivity dimension $D_{\mathcal{T}}$ varies rather similar compared to the Kaplan–Yorke

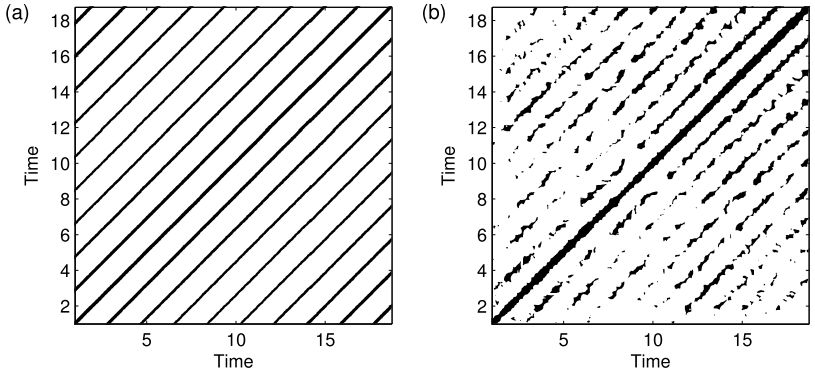

Fig. 4. Recurrence plots of the Lorenz96 system $x_k(t)$ for $f = 5$ and system size of (a) $N = 38$ and (b) $N = 47$, showing periodic and chaotic dynamics.

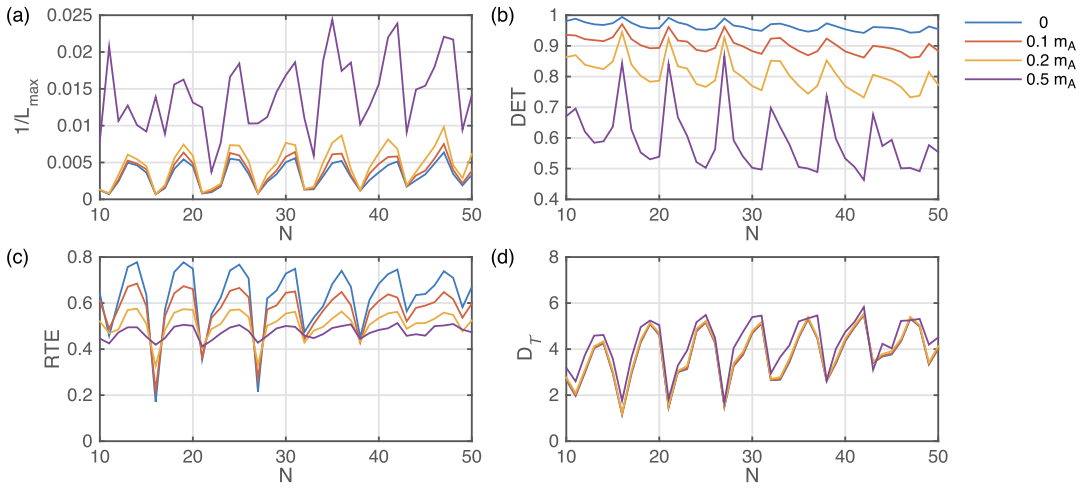

Fig. 5. Influence of noise on the RQA results. Observational, normally distributed noise is added to the time series of the Lorenz96 system. The standard deviation of the noise is relative to the averaged mean amplitude m_A of the time series.

dimension D_{KY}. It also shows the upward trend with increasing N (Fig. 3(c)), but D_{KY} is in average 2.5 times higher than $D_{\mathcal{T}}$. The correlation of D_{KY} with DET and $D_{\mathcal{T}}$ is -0.715 and 0.723, respectively.

The recurrence based measures are able to reveal the dynamics using very short time series of length 1500, obtained from 3000 iterations, in comparison to the classic measures where 200,000 iterations and the differential equations had been necessary. One explanation is that an RP compares the states at all time points with those at all other time points (i.e., an N^2 pair-wise test), and that the measures are of statistical nature. The method will also work up to a certain level of noise. In the following we investigate the influence of noise by adding normally distributed random numbers to the time series. The standard deviation of the noise is chosen relative to the mean amplitude m_A of the time series and is varied between 0 (no noise) and $0.5 \times m_A$. We find that even for a large portion of noise with standard deviation half of the mean amplitude, the RQA measures distinguish clearly between the different dynamics (Fig. 5). In particular, $D_{\mathcal{T}}$ shows almost identical results for the considered noise levels (Fig. 5(d)). With increasing noise, DET and RTE decrease, and $1/L_{\max}$ increases. However, there are differences in their variations with respect to the noise level. As the variation of DET and $1/L_{\max}$ increases for growing noise (Fig. 5(b,d)), the variation for RTE decreases (Fig. 5(c)). It is remarkable that $D_{\mathcal{T}}$ is the measure with the lowest sensitivity on noise, whereas $1/L_{\max}$ is less sensitive for low noise levels but becomes abruptly high sensitive for high noise levels (Fig. 5(a)). Nevertheless, these results suggest that the approach is quite robust even for higher level of observational noise (at least for differentiating chaotic and periodic dynamics).

5. Application on satellite time series imagery

In order to illustrate the applicability of the proposed RP quantitative measures on spatially extended and potentially high-dimensional real world data, we use MODIS satellite time series imagery of the extended vegetation index (EVI) of two test sites in NE Spain, centre coordinates 42.37°N, 0.51°E, and NE Brazil, 5.00°S, 39.50°W (Fig. 6). The test sites are characterized by differently complex vegetation dynamics both in the temporal (inter-annual and intra-annual) and spatial domain (Fig. 7) as a result of diverse natural processes and human interactions [38,39]. Thus, these sites are seen as ideal to study the usefulness of the proposed RP measures in order to objectively quantify and evaluate this complex behavior and decipher changes in vegetation cover dynamics related to land extensification/intensification or climate change and drought. The subhumid Spanish test site shows a pronounced seasonal variation in precipitation and temperature with cold and dry winters and hot and stormy summers, whereas the Brazilian test site located in the so-called drought polygon is characterized by a semiarid climate with distinct dry and wet seasons and rainfall of high temporal and spatial irregularity. The Spanish test site has undergone severe land use changes during the last 50 years with the abandoning of former agricultural areas and subsequent reforestation as well as setting aside of lands from agriculture promoted by the European Agricultural Policy [40]. The Brazilian test site has been more intensively occupied since 1985, when the Federal Government accomplished a land reform leading to the intensification of agricultural and livestock practices. A dense water surface reservoir network has been built in the last decades to mitigate water scarcity problems [41].

The MODIS-Terra MOD13Q1 product used for this real world application is a 16-day composite image of the enhanced vegetation index (EVI) in a sinusoidal projection with a spatial resolution of 250 m. Global MODIS vegetation indices are designed to provide consistent spatial and temporal datasets used for global monitoring of vegetation conditions. The EVI is chosen since it minimizes canopy background variations and maintains sensitivity over dense vegetation. We obtained 316 MOD13Q1 images for the period February 2000 to November 2013 for both the MODIS tiles h18v04 (Spain) and h14v09 (Brazil) from the Land Processes Distributed Active Archive Center (LP DAAC), located at the US Geological Survey (USGS) Earth Resources Observation and Science (EROS) Center (`lpdaac.usgs.gov`).

In both regions we consider subareas of 5×5 km^2 ($N = 441$ grid points) varying around the centre point by 0.25° and within a range of [−0.5° 0.5°] (resulting in 25 subareas for both regions). That way, the subareas contain a mixture of land covers representative for the test sites. For calculating the RP, we create the phase space vector $\vec{x}$ from the pixels of the satellite image subarea, i.e., $\vec{x}$ has 441 dimensions (not to be confused with the dimension of the dynamics).

For both regions we visually find periodic patterns in the corresponding RPs, revealing mainly the seasonal variability (Fig. 8). The appearance of the periodic patterns differ for Spain (more line-like patterns) and Brazil (more block-like patterns), indicating substantial differences in the spatial dynamics. The RP quantification by the measures DET, $1/L_{\max}$, and $D_{\mathcal{T}}$ clearly reveals quantitative differences: in Brazil we find a more erratic or chaotic spatio-temporal pattern than in Spain, indicated by lower DET and higher

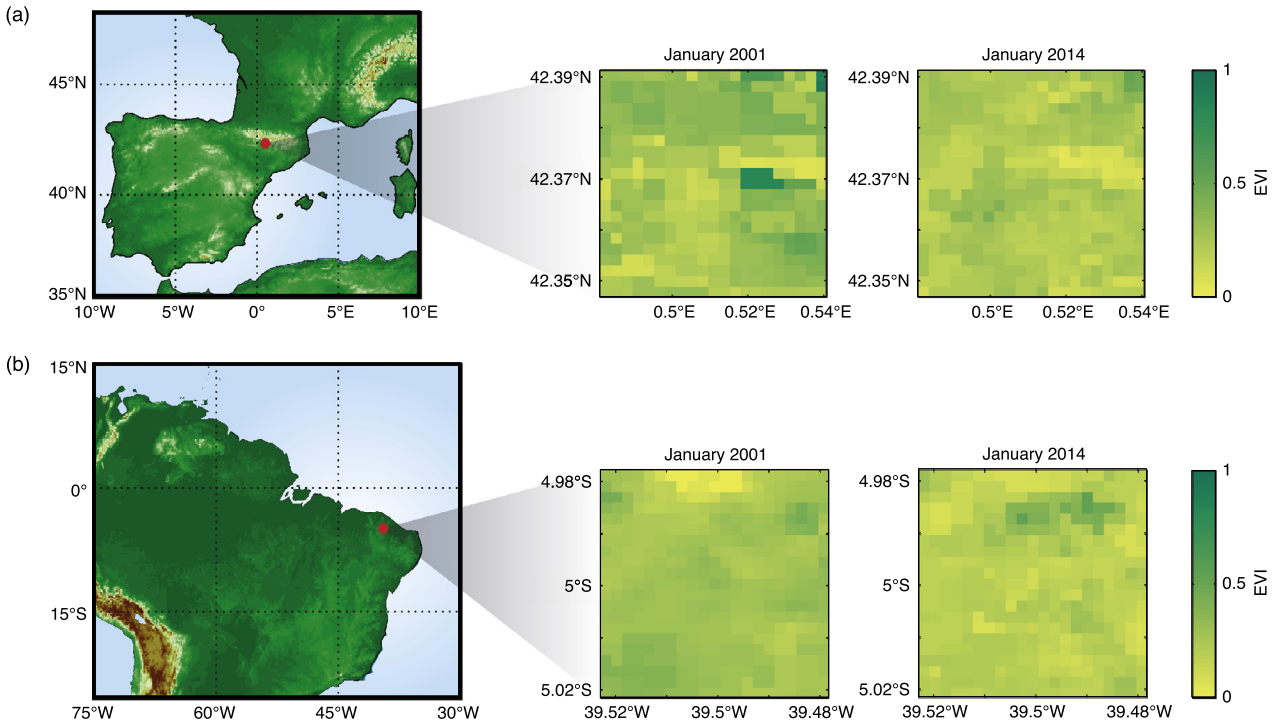

Fig. 6. Geographical location and MODIS extended vegetation index (EVI) within the 5×5 km^2 subarea used for the analysis for the regions (a) NE Spain and (b) NE Brazil.

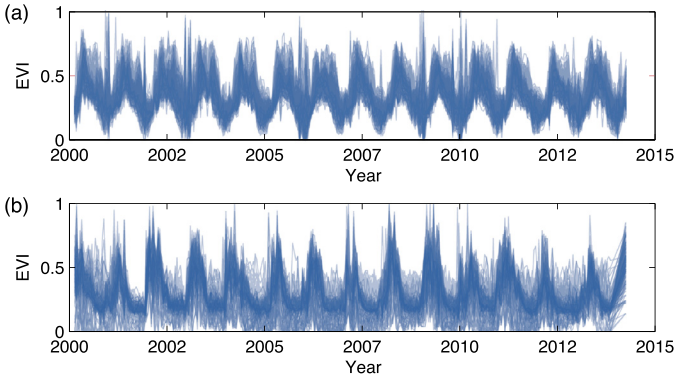

Fig. 7. EVI time series of all pixels in the subareas as shown in Fig. 6 for (a) NE Spain and (b) NE Brazil. The vegetation dynamics in NE Brazil appears clearly to be more erratic in the temporal and spatial domain than in NE Spain.

$1/L_{\max}$ as well as $D_{\mathcal{T}}$ for Brazil (Fig. 9, Table 1). Although the considered subareas consist of information that is a mixed signal of several land cover classes, the difference between Spain and Brazil is consistent for subareas of varying location. These results can be interpreted in such sense that the vegetation (or land use) dynamics in Brazil is probably less regulated and less predictable than in Spain.

6. Conclusion

By using the Lorenz96 model as a prototypical example of spatially extended dynamics with large degrees of freedom, we have shown that recurrence plot based analysis can be used to investigate high-dimensional dynamics from rather short time series and provides insights in the fundamental features of the dynamics, comparable with the Kaplan–Yorke dimension or the Lyapunov exponent. This study, thus, answers the hitherto open question, whether recurrence plots and their quantification are suitable to study high-dimensional chaos. The more systematic study on the limits of the used methods and the necessary length of time series in dependence on the degrees of freedom of the system is a subject of future work.

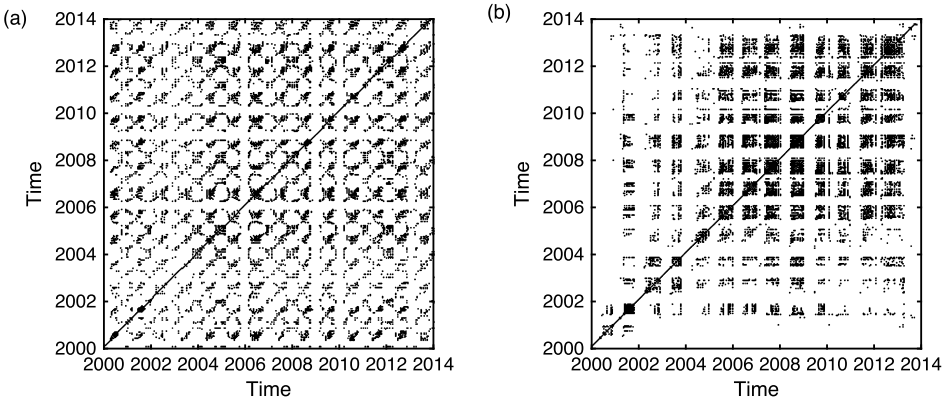

Fig. 8. Recurrence plot of a 5×5 km^2 subarea of the EVI of test sites in (a) NE Spain and (b) NE Brazil. The selected subarea is situated at the centre point of the study region (see text).

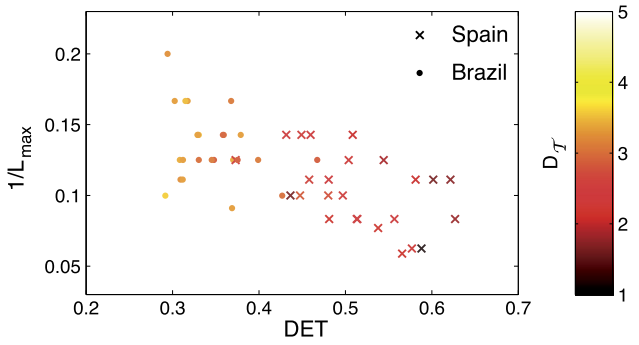

Fig. 9. Recurrence quantification measures for the MODIS EVI data for different subareas around the study regions' centre point.

Table 1
Median of recurrence quantification measures for the MODIS EVI data (standard deviation in brackets).

	Spain	Brazil
DET	0.51 (0.07)	0.33 (0.04)
$1/L_{\max}$	0.10 (0.03)	0.13 (0.03)
$D_{\mathcal{T}}$	2.35 (0.45)	3.85 (0.41)

Moreover, by applying the method to MODIS satellite time series data we have demonstrated its suitability for the investigation of extended spatio-temporal dynamics of real world processes. The recurrence analysis has indicated a clear difference in the spatio-temporal vegetation dynamics in a subhumid (Spain) and in a semiarid (Brazil) climate, where the first shows a more regular pattern, whereas the latter is characterized by a more irregular and less predictable behavior.

Acknowledgements

We acknowledge support from the DFG and FAPESP (projects MA 4759/4-1 and IRTG 1740/TRP 2011/50151-0) and from the Government of the Russian Federation (Agreement No. 14.Z50.31.0033).

References

[1] J.-P. Eckmann, S. Oliffson Kamphorst, D. Ruelle, Recurrence plots of dynamical systems, Europhys. Lett. 4 (9) (1987) 973–977, http://dx.doi.org/10.1209/0295-5075/4/9/004.
[2] N. Marwan, A historical review of recurrence plots, Eur. Phys. J. Spec. Top. 164 (1) (2008) 3–12, http://dx.doi.org/10.1140/epjst/e2008-00829-1.
[3] N. Marwan, M.C. Romano, M. Thiel, J. Kurths, Recurrence plots for the analysis of complex systems, Phys. Rep. 438 (5–6) (2007) 237–329, http://dx.doi.org/10.1016/j.physrep.2006.11.001.
[4] R.V. Donner, J. Heitzig, J.F. Donges, Y. Zou, N. Marwan, J. Kurths, The geometry of chaotic dynamics – a complex network perspective, Eur. Phys. J. B 84 (2011) 653–672, http://dx.doi.org/10.1140/epjb/e2011-10899-1.
[5] C.L. Webber Jr., N. Marwan, Recurrence Quantification Analysis – Theory and Best Practices, Springer, Cham, 2015.
[6] N. Marwan, J.F. Donges, Y. Zou, R.V. Donner, J. Kurths, Complex network approach for recurrence analysis of time series, Phys. Lett. A 373 (46) (2009) 4246–4254, http://dx.doi.org/10.1016/j.physleta.2009.09.042.
[7] G. Litak, M. Wiercigroch, B.W. Horton, X. Xu, Transient chaotic behaviour versus periodic motion of a parametric pendulum by recurrence plots, Z. Angew. Math. Mech. 90 (1) (2010) 33–41, http://dx.doi.org/10.1002/zamm.200900290.
[8] O. Kopáček, V. Karas, J. Kovář, Z. Stuchlík, Transition from regular to chaotic circulation in magnetized coronae near compact objects, Astrophys. J. 722 (2) (2010) 1240, http://dx.doi.org/10.1088/0004-637X/722/2/1240.
[9] Z.O. Guimarães-Filho, I.L. Caldas, R.L. Viana, I.C. Nascimento, Y.K. Kuznetsov, J. Kurths, Recurrence quantification analysis of turbulent fluctuations in the plasma edge of Tokamak Chauffage Alfvén Brésilien tokamak, Phys. Plasmas 17 (2010) 012303, http://dx.doi.org/10.1063/1.3280010.
[10] G.M. Ramírez Ávila, A. Gapelyuk, N. Marwan, T. Walther, H. Stepan, J. Kurths, N. Wessel, Classification of cardiovascular time series based on different coupling structures using recurrence networks analysis, Philos. Trans. R. Soc. Lond. A 371 (1997) (2013) 20110623, http://dx.doi.org/10.1098/rsta.2011.0623.
[11] D.C. Richardson, R. Dale, Looking to understand: the coupling between speakers' and listeners' eye movements and its relationship to discourse comprehension, Cogn. Sci. 29 (6) (2005) 1045–1060.
[12] E.D. Eneyew, M. Ramulu, Tool wear monitoring using microphone signals and recurrence quantification analysis when drilling composites, in: Advanced Materials Research, vol. 711, 2013, pp. 239–244.
[13] M. Tahmasebpour, R. Zarghami, R. Sotudeh-Gharebagh, N. Mostoufi, Characterization of various structures in gas–solid fluidized beds by recurrence quantification analysis, Particuology 11 (6) (2013) 647–656, http://dx.doi.org/10.1016/j.partic.2012.08.005.
[14] B. Krese, M. Perc, E. Govekar, Experimental observation of a chaos-to-chaos transition in laser droplet generation, Int. J. Bifurcation Chaos 21 (6) (2011) 1689–1699, http://dx.doi.org/10.1142/S0218127411029367.
[15] I. Konvalinka, D. Xygalatas, J. Bulbulia, U. Schjodt, E.M. Jegindo, S. Wallot, G. Van Orden, A. Roepstorff, Synchronized arousal between performers and related spectators in a fire-walking ritual, Proc. Natl. Acad. Sci. 108 (20) (2011) 8514–8519, http://dx.doi.org/10.1073/pnas.1016955108.
[16] J.F. Donges, R.V. Donner, M.H. Trauth, N. Marwan, H.J. Schellnhuber, J. Kurths, Nonlinear detection of paleoclimate-variability transitions possibly related to human evolution, Proc. Natl. Acad. Sci. 108 (51) (2011) 20422–20427, http://dx.doi.org/10.1073/pnas.1117052108.
[17] D.B. Vasconcelos, S.R. Lopes, R.L. Viana, J. Kurths, Spatial recurrence plots, Phys. Rev. E 73 (2006) 056207, http://dx.doi.org/10.1103/PhysRevE.73.056207.
[18] N. Marwan, J. Kurths, P. Saparin, Generalised recurrence plot analysis for spatial data, Phys. Lett. A 360 (4–5) (2007) 545–551, http://dx.doi.org/10.1016/j.physleta.2006.08.058.
[19] T.L. Prado, P.P. Galuzio, S.R. Lopes, R.L. Viana, Spatial recurrence analysis: a sensitive and fast detection tool in digital mammography, Chaos 24 (2014) 013106, http://dx.doi.org/10.1063/1.4861895.
[20] Z.O. Guimarães-Filho, I.L. Caldas, R.L. Viana, J. Kurths, I.C. Nascimento, Y.K. Kuznetsov, Recurrence quantification analysis of electrostatic fluctuations in fusion plasmas, Phys. Lett. A 372 (7) (2008) 1088–1095, http://dx.doi.org/10.1016/j.physleta.2007.07.088.
[21] C. Mocenni, A. Facchini, A. Vicino, Identifying the dynamics of complex spatio-temporal systems by spatial recurrence properties, Proc. Natl. Acad. Sci. 107 (18) (2010) 8097–8102, http://dx.doi.org/10.1073/pnas.0910414107.
[22] J.-P. Eckmann, D. Ruelle, Ergodic theory of chaos and strange attractors, Rev. Mod. Phys. 57 (3) (1985) 617–656, http://dx.doi.org/10.1103/RevModPhys.57.617.
[23] P. Grassberger, I. Procaccia, Measuring the strangeness of strange attractors, Physica D 9 (1–2) (1983) 189–208, http://dx.doi.org/10.1016/0167-2789(83)90298-1.
[24] J.-P. Eckmann, D. Ruelle, Fundamental limitations for estimating dimensions and Lyapunov exponents in dynamical systems, Physica D 56 (2–3) (1992) 185–187, http://dx.doi.org/10.1016/0167-2789(92)90023-G.
[25] E.N. Lorenz, Predictability: A Problem Partly Solved, vol. 1, ECMWF, Reading, UK, 1996, pp. 1–18.
[26] E.N. Lorenz, K.A. Emanuel, Optimal sites for supplementary weather observations: simulation with a small model, J. Atmos. Sci. 55 (3) (1998) 399–414, http://dx.doi.org/10.1175/1520-0469(1998)055<0399:OSFSWO>2.0.CO;2.
[27] D. Pazó, I.G. Szendro, J.M. López, M.A. Rodríguez, Structure of characteristic Lyapunov vectors in spatiotemporal chaos, Phys. Rev. E 78 (1) (2008) 016209, http://dx.doi.org/10.1103/PhysRevE.78.016209.
[28] A. Karimi, M.R. Paul, Extensive chaos in the Lorenz-96 model, Chaos 20 (4) (2010) 043105, http://dx.doi.org/10.1063/1.3496397.
[29] F. Christiansen, H.H. Rugh, Computing Lyapunov spectra with continuous Gram–Schmidt orthonormalization, Nonlinearity 10 (5) (1997) 1063–1072, http://dx.doi.org/10.1088/0951-7715/10/5/004.
[30] K. Ramasubramanian, M. Sriram, A comparative study of computation of Lyapunov spectra with different algorithms, Physica D 139 (1–2) (2000) 72–86, http://dx.doi.org/10.1016/S0167-2789(99)00234-1.
[31] E.J. Ngamga, D.V. Senthilkumar, A. Prasad, P. Parmananda, N. Marwan, J. Kurths, Distinguishing dynamics using recurrence-time statistics, Phys. Rev. E 85 (2) (2012) 026217, http://dx.doi.org/10.1103/PhysRevE.85.026217.
[32] M.A. Little, P.E. McSharry, S.J. Roberts, D.A.E. Costello, I.M. Moroz, Exploiting nonlinear recurrence and fractal scaling properties for voice disorder detection, Biomed. Eng. Online 6 (23) (2007) 1–19, http://dx.doi.org/10.1186/1475-925X-6-23.
[33] V.S. Anishchenko, S.V. Astakhov, Poincaré recurrence theory and its applications to nonlinear physics, Phys. Usp. 56 (10) (2013) 955–972, http://dx.doi.org/10.3367/UFNe.0183.201310a.1009.
[34] Y. Zou, R.V. Donner, J.F. Donges, N. Marwan, J. Kurths, Identifying complex periodic windows in continuous-time dynamical systems using recurrence-based methods, Chaos 20 (4) (2010) 043130, http://dx.doi.org/10.1063/1.3523304.

[35] P. Grassberger, I. Procaccia, Characterization of strange attractors, Phys. Rev. Lett. 50 (5) (1983) 346–349, http://dx.doi.org/10.1103/PhysRevLett.50.346.

[36] N. Marwan, How to avoid potential pitfalls in recurrence plot based data analysis, Int. J. Bifurcation Chaos 21 (4) (2011) 1003–1017, http://dx.doi.org/10.1142/S0218127411029008.

[37] N. Marwan, M. Riley, A. Giuliani, C.L. Webber Jr., Translational Recurrences – From Mathematical Theory to Real-World Applications, vol. 103, Springer, Cham, 2014.

[38] H.A. Barbosa, A.R. Huete, W.E. Baethgen, A 20-year study of NDVI variability over the Northeast Region of Brazil, J. Arid Environ. 67 (2) (2006) 288–307, http://dx.doi.org/10.1016/j.jaridenv.2006.02.022.

[39] J. Hill, M. Stellmes, T. Udelhoven, A. Röder, S. Sommer, Mediterranean desertification and land degradation. Mapping related land use change syndromes based on satellite observations, Glob. Planet. Change 64 (2008) 146–157, http://dx.doi.org/10.1016/j.gloplacha.2008.10.005.

[40] T. Lasanta, S.M. Vicente-Serrano, Complex land cover change processes in semiarid Mediterranean regions: an approach using Landsat images in northeast Spain, Remote Sens. Environ. 124 (2012) 1–14, http://dx.doi.org/10.1016/j.rse.2012.04.023.

[41] C.E. de Toledo, J.C. de Araújo, C.L. de Almeida, The use of remote-sensing techniques to monitor dense reservoir networks in the Brazilian semiarid region, Int. J. Remote Sens. 35 (10) (2014) 3683–3699, http://dx.doi.org/10.1080/01431161.2014.915593.